Tetrahedron xxx (xxxx) xxx

Contents lists available at ScienceDirect

Tetrahedron

journal homepage: www.elsevier.com/locate/tet

Engineering aromatic heterocycle strategy: Improving copper electrodeposition performance via tuning the bandgap of diketopyrrolopyrrole-based leveler

Kang Wang, Jinming Feng, Jie Xu, Jun Li, Maria Mai, Xiaomin Wang, Limin Wang*

Key Laboratory for Advanced Materials, Institute of Fine Chemical, School of Chemistry & Molecular Engineering, East China University of Science and Technology, 130 Meilong Road, Shanghai, 200237, China

A R T I C L E I N F O

Article history:
Received 22 October 2019
Received in revised form
9 December 2019
Accepted 12 December 2019
Available online xxx

Keywords:
Bandgap
Diketopyrrolopyrroles
Electroplating
Leveler
Quaternary ammonium salts

A B S T R A C T

The bandgap of organics is an important descriptor to evaluate the interface adhesion of an organic agent on metal surface. However, insight into the role of chalcogens tuning of π-conjugated materials in influencing the bandgap is still deficient. Here, a family of diketopyrrolopyrrole(DPP)-based quaternary ammonium salts containing different chalcogens are innovatively synthesized through bottom-up strategy and served as new levelers in conformal copper electrodeposition. The photophysical and electrochemical properties including cyclic voltammetry (CV),potentiodynamic polarization curves and galvanostatic measurements (GMs) of those compounds were tested. Compared with other counterparts, SeDPP-QAS presents the narrowest bandgap showing great potential in conformal copper electrodeposition. Through-hole electroplating test and the scanning electron microscope (SEM) images of coating layer demonstrate that bandgap tuning is an efficient method to level and regulate the electrodeposition performance. Besides, theoretical calculations and X-ray photoelectron spectroscopy (XPS) were applied detect the adsorption mechanism between organic agent and copper surface. This work broadens the understanding of bandgap engineering of organics in copper electrodeposition, and provides guidance for the future design of organic materials in adsorbing other metal-based materials.

© 2019 Elsevier Ltd. All rights reserved.

1. Introduction

Copper electrodeposition is widely used in printed circuit boards (PCBs), integrated circuit (IC) package and cutting-edge microprocessors since the metallic copper has good electrical conductivity, thermal conductivity and corrosion resistance [1–4]. Acid bright copper plating is the most important method for copper electrodeposition, its characteristics are as follows: the composition of the plating solution are simple copper sulfate and sulfuric acid [5]; the plating solution has high current efficiency and high deposition speed; the brightening effect of the brightener is obvious and the specular gloss coating can be obtained [6]. In order to gain a coating with good appearance, qualified leveling performance and excellent physical properties, various organic additives must be added to the plating solution, including inhibitor, brighter and leveler [7,8]. Among them, the leveler is an important organic additive serving as a kind of additive that could selectively adsorb in the high current density or strong mass flux area to level and regulate the coating performance during copper electrodeposition process. So far, only a few leveling agents have been reported, such as Janus Green B (JGB), diazine black, methylene blue, alcian blue and branched quaternary ammonium salts (QAS) [9,10]. Wang et al. demonstrated that the narrow bandgap of JGB could exert strong adsorption on cathodic surface and favorable inhibition of cooper electrodeposition on the cathode [11]. Moreover, Wang et al. studied the bandgap and electrostatic potential (ESP) differences between JGB and other leveler of polymerizates of imidazole and epichlorohydrin (IMEP), the IMEP leveler possesses larger bandgap but showing higher ESP which presents better plating performance [5]. Systematically studied the structure-performance relationship of leveler is still a great challenge, insight into the bandgap of leveler is still deficient.

Diketopyrrolopyrroles (DPPs) as one of the most researched groups of organic pigments have attracted tremendous interests because of their outstanding physical and chemical properties [12]. DPP derivatives could be functionalized as fluorescent sensor

* Corresponding author.
E-mail address: wanglimin@ecust.edu.cn (L. Wang).

https://doi.org/10.1016/j.tet.2019.130882
0040-4020/© 2019 Elsevier Ltd. All rights reserved.

because of their intense fluorescence after the deprotonation of lactam bond and rich modification sites [13–16]. They also can be used as optoelectronic device applications including organic field effect transistors (OFETs), organic solar cells (OSCs), organic light-emitting diodes (OLEDs) owing to the excellent properties of the thermal and photostability [17–24], planarity of the chromophore and ambipolar charge carrier transport. The planarity and electron-deficient pyrrole site of DPP dyes are exactly what the leveling agent needs, the planar electron-deficient region may exert selective adsorption on high current density cathode surface and leveling the deposition behavior. Unfortunately, the strong intermolecular hydrogen bond and π-π stacking properties lead to poor water solubility that impedes the usage of DPP pigments as leveler in copper electroplating. In our previous work, the strategy of quaternary ammonium salt was introduced to significantly enhance the water solubility of Cl-DPP (Chlorine substituted DPP) via grafted on amide site and successfully applied into printed circuit boards (PCBs) electroplating [25]. Afterwards, the aryl-modification strategy was proposed to enhance the adsorption performance of DPP-based levelers [26]. However, the structure-performance correlation is not clear and the mentioned aryl-modification strategy is not very satisfactory because the most effective leveler CF_3-DPP (trifluoromethyl substituted DPP) still shows relative larger bandgap.

Herein, the bandgap engineering strategy was proposed by substituting the conventional aryl groups of DPP with varies of heterocycles of to obtain the more efficient leveler with smaller bandgap. To be specific, four DPP-based quaternary ammonium salts (compounds p-ClDPP-QAS, FDPP-QAS, TDPP-QAS and SeDPP-QAS) were designed and synthesized with different aromatic rings of DPP skeletons as levelers in copper electroplating [27]. The electrochemical behaviors of these DPP derivatives were also characterized by a series of electrochemical tests containing Galvanostatic measurements (GMs), Cyclic voltammetry (CV) and potentiodynamic polarization curves to analyze the effects of additives on cathodic polarization. Besides, the wetting performance of four DPP derivatives were evaluated by contact angle. The results show that the inhibiting abilities of FDPP-QAS, TDPP-QAS and SeDPP-QAS on copper electrodeposition increasingly improve and these three novel levelers are all better than the previously reported p-ClDPP-QAS [19]. To explain why there are different inhibiting abilities of each derivative, contact angle, XPS and quantum chemical calculation were carried out. The electronic properties and molecule orbital information well explained the inhibiting ability. According to these measurements, SeDPP-QAS was chosen as representative leveler for through-holes electroplating process to evaluate the practical leveling performance. In addition, its influence on the surface morphology was also investigated by field-emission scanning electron microscopy (FE-SEM) and X-ray diffraction (XRD).

2. Experimental

2.1. Synthesis of the additives

The DPP derivatives with different aromatic ring units at 3 and 6 positions of the pyrrolopyrrole core were synthesized from an aryl or heteroaryl nitrile (Ar-CN) and succinate. The synthesis routes are shown in Scheme 1. p-ClDPP was prepared according to the synthetic methodology reported in the previous literature [20]. The presence of space steric caused by benzene ring at the 3 and 6 positions of the DPP core enhances the repulsive interaction with the adjacent lactam ring resulting in a distorted molecular geometry [28]. In order to attain a highly co-planar molecular backbone for efficient π-π stacking, we introduced five membered heterocyclic units onto DPP to alleviate this twisted geometry [29], so the DPP derivatives with furan and thiophene units were synthesized and at the same time the effect of selenium in lowering the lowest unoccupied molecular orbitals (LUMOs) energy level was also explored [30,31]. Moreover, the decrease in the bandgap also can be attributed to the decrease in aromaticity and an increase in quinoidal character in the selenophene derivative [31]. TDPP was synthesized following the reported literature [12], selenophene-2-carbonitrile was prepared as described by Martin Heeney [30]. The synthetic route of selenophene-2-carbonitrile reaction with diethyl succinate in the presence of sodium is the same with TDPP. The obtained deep red DPP derivatives had low solubility because of the strong intermolecular interactions between the N–H and C=O groups. The alkyl chains were connected to the nitrogen atoms of the DPP unit in the presence of CH_3CN with 1,6-dibromohexane and potassium tert-butoxide at 80 °C. After the N-alkylation, the obtained four DPP derivatives were done further reacted with the quaternary ammonium salts at the temperature of 80 °C, with CH_3CN as solvent, $NMe_3 \cdot HCl$ as nucleophilic reagent and $NaHCO_3$ as base. After that, the column chromatogram was carried out to purify the crude product then the target products (p-ClDPP-QAS, FDPP-QAS, TDPP-QAS and SeDPP-QAS) were given and the main synthetic routes are shown in Scheme 1. The detailed synthetic routes and characterization are provided in the supporting information.

2.2. Characterization

^1H NMR and ^{13}C NMR spectra were recorded with a Bruker Avance 400 spectrometer at 400 MHz and 100 MHz respectively. Tetramethylsilane was used as an internal reference and $CDCl_3$ or CD_3OD as a solvent. The chemical shifts (δ) and coupling constants (*J*) were expressed in parts per million and hertz, respectively. A Micromass GCTTM mass spectrometer was used to record the mass (see the Supporting Information) spectra. Chemicals were commercially available and used without purification. Chromatography: column chromatography was performed with silica gel or aluminum oxide, AR, neutral (200–300 mesh ASTM). Contact angle was tested by Shanghai Zhong Chen Contact Angle Measuring Instrument (JC2000D). A PGSTAT302N (Auto-Lab) was used for all electrochemical tests. Plating performances were evaluated by the cross-section images detected by field-emission scanning electron microscopy (FE-SEM, Hitachi S3400-N). Photoluminescence spectra were examined using a Varian Cary Eclipse spectrophotometer. Absorption spectra were measured on a Thermo UV–Vis spectrophotometer. XPS were tested by Rotating Anode X-ray Powder Diffractometer(18KW/D/max2550VB/PC).

2.3. Electrochemical measurements

We used a 3 mm diameter platinum rotating disk electrode (Pt-RDE) as a base for the working electrode (WE). A Pt stick with a diameter of 2 mm was used as counter electrode (CE), and a silver/silver chloride electrode (Ag/AgCl) was served as the reference electrode (RE). The composition of the base electrolyte was 60 mg/L NaCl, 60 g/L $CuSO_4 \cdot 5H_2O$ and 200 g/L H_2SO_4 for all electrochemical tests. Polyethylene glycol (PEG, MW = 10000, SIGMA), NaCl (Fisher, Certified ACS), and bis(3-sulfopropyl) disulfide (SPS; Jiangsu Mengde New Materials Technology Co., Ltd.) were additives. The four DPP derivatives used as levelers in this work were p-ClDPP-QAS, FDPP-QAS, TDPP-QAS, and SeDPP-QAS, respectively.

A constant scan rate of 50 mV/s was used for cyclic voltammetry experiments. The domain of study ranged from 1.57 to 0.20 V. A thin copper layer with a thickness of 500 nm was pre-deposited onto the Pt-RDE in a pre-deposition bath before each

Please cite this article as: K. Wang et al., Engineering aromatic heterocycle strategy: Improving copper electrodeposition performance via tuning the bandgap of diketopyrrolopyrrole-based leveler, Tetrahedron, https://doi.org/10.1016/j.tet.2019.130882

ARTICLE IN PRESS

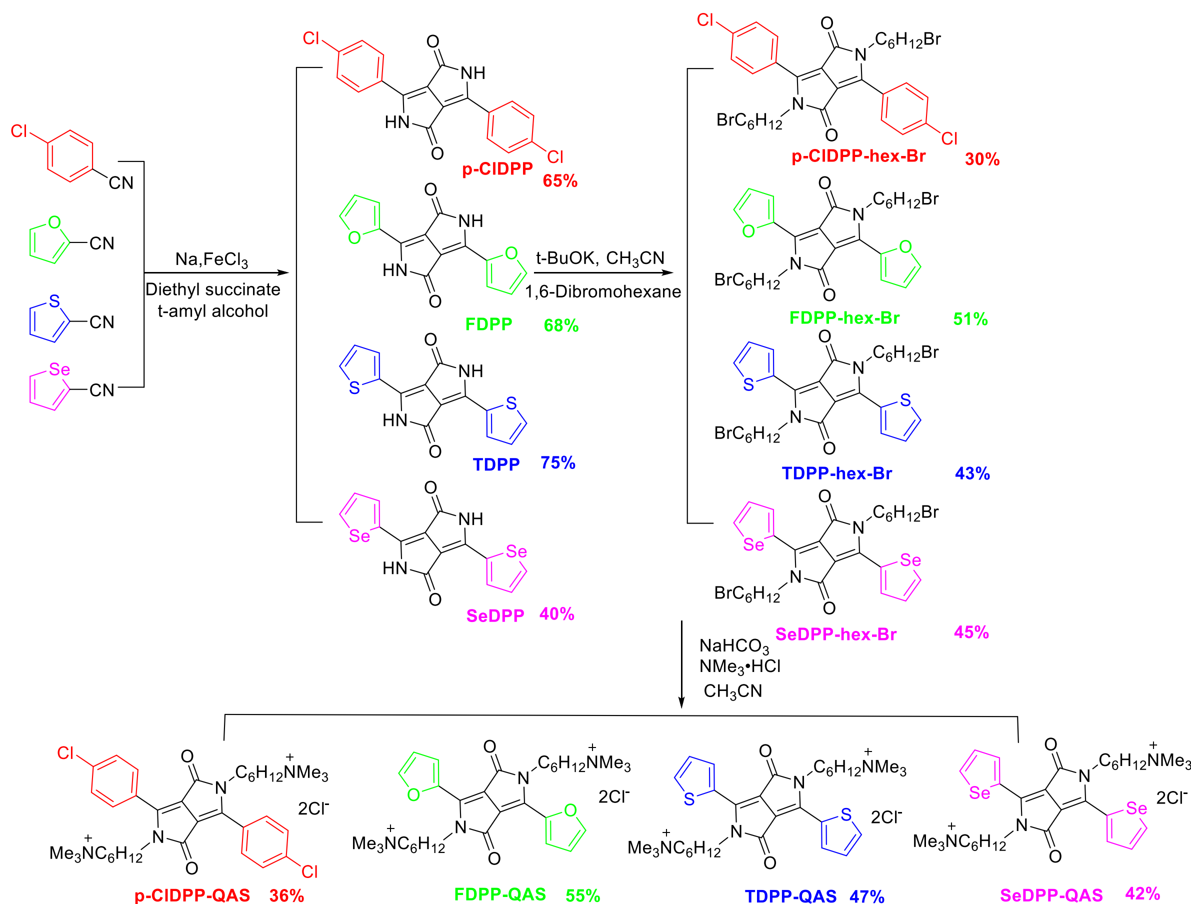

Scheme 1. The synthesis of DPP derivatives with varied donor units.

potentiodynamic polarization test and galvanostatic measurements (GMs). The pre-deposition bath only contained 60 g/L $CuSO_4 \cdot 5H_2O$ and 200 g/L H_2SO_4 to prepare a Cu-RDE. A constant scan rate of 20 mV/s was used in the potentiodynamic polarization test, which scanned from 0 to 0.8 V. The GMs were carried out using the Cu-RDE at a current density of 1.5 A/dm^2. After pre-plating at −0.15 V for 5 min.

2.4. Electroplating

A 15 × 5 cm^2 PCB fragments with many through-holes (THs) were used as test samples for TH electroplating. The diameter and depth of TH were 250 μm and 3 mm, respectively. The phosphorus-containing copper plate was used as the anode and directly placed in the Haring cell with a 1500 mL working volume. The PCB fragments were plated at a current density of 1.5 A/dm ^{2} for 70 min at 25 °C. In order to ensure good mass transfer, a continuous air bubble flow is adopted during electroplating process. Throwing power (TP) is the most important indicator for leveling performance of the leveler, TP is defined in Scheme S1 and calculated by equation (1) shown in supporting information.

2.5. Calculation methods

B3LYP/6-311G (d, p) methods were used to fully optimize the geometries of all the quaternary ammonium salts in this study [32,33]. Frequency calculations were carried out at the same theoretical levels to make sure that all the structures were genuine minima on the potential energy surface. We used the molecular orbital to analysis the quaternary ammonium salts. The contour surfaces of the highest occupied molecular orbitals (HOMOs) and lowest unoccupied molecular orbitals (LUMOs) were represented. The Gaussian 09 suite of programs was used for all of the calculations [34]. And Gaussiview program was used for visualization of the electrostatic potential (ESP), which mapped the distribution of electron density in the molecular [35,36].

3. Results and discussion

The bandgap engineering strategy is proposed by tuning the aryl ring to heterocyclic ring of DPP-based quaternary ammonium salt to obtain more efficient leveler with smaller bandgap [37]. Therefore, three DPP-based quaternary ammonium salts (compounds FDPP-QAS, TDPP-QAS and SeDPP-QAS) with different heterocyclic rings instead of previously investigated chlorobenzene, p-ClDPP-QAS, attached to DPP skeletons as levelers in copper electroplating are designed and synthesized. The magnetic resonance spectroscopy and mass spectrometry were shown in supplemental material.

3.1. Electrochemical evaluation

Firstly, as shown in Fig. 1a, the cyclic voltammograms (CV) was investigated in the condition of with and without different DPP quaternary ammonium salts (2 μmol/L). The CV tests reveal that DPP quaternary ammonium salts can inhibit the copper deposition

Please cite this article as: K. Wang et al., Engineering aromatic heterocycle strategy: Improving copper electrodeposition performance via tuning the bandgap of diketopyrrolopyrrole-based leveler, Tetrahedron, https://doi.org/10.1016/j.tet.2019.130882

ARTICLE IN PRESS

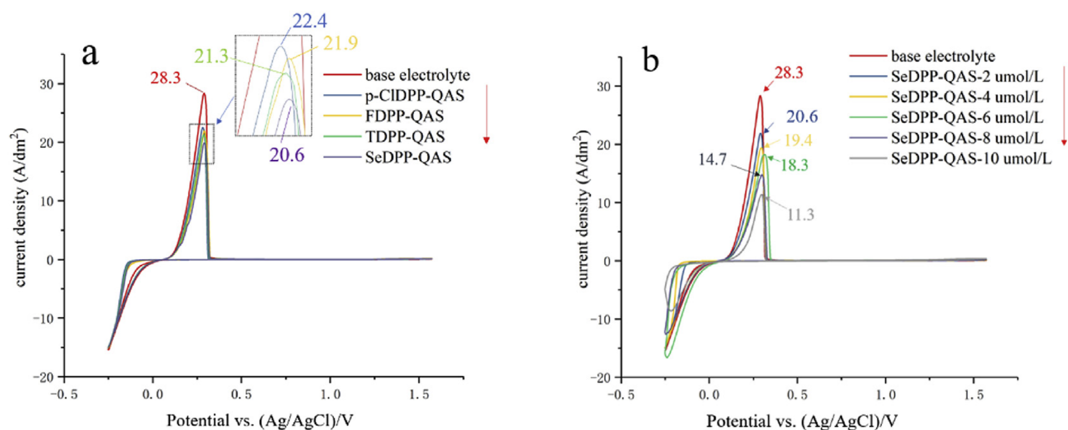

Fig. 1. (a) Cyclic voltammograms containing no additives and 2 μmol/L DPP derivatives p-ClDPP-QAS,FDPP-QAS,TDPP-QAS and SeDPP-QAS in base electrolyte. (b) Cyclic voltammograms containing no additives and SeDPP-QAS of different concentration gradient (2 μmol/L,4 μmol/L,6 μmol/L, 8 μmol/L, 10 μmol/L) in base electrolyte. The electrode rotation speed is 1000 rpm.

and the suppressing behavior of SeDPP-QAS is better than other three quaternary ammonium salts at a concentration of 2 μmol/L. Further, the effect of concentration exerting on suppressing behaviors is studied using representative additive SeDPP-QAS as prototype (Fig. 1b). Specifically, the oxidized areas and peak current densities decrease with the increasing concentration of SeDPP-QAS, and the peak current density down to 11.3 A/dm^2 upon 10 μmol/L concentration of SeDPP-QAS injected into the electrolyte.

Galvanostatic measurements (GMs) were applied to understand the interactions between the suppresser (i.e., PEG), the accelerator (i.e., SPS) and the as-synthesized DPP-based levelers. Surprisingly, as shown in Fig. 2, DPP-based levelers have different synergistic interaction with other electroplating additives. The GMs with different rotation speeds of Cu-RDE are studied, the SeDPP-QAS exerted the greatest inhibiting effect among the four synthesized levelers. Here, two different rotating speeds (1000 & 100 rpm) were conducted to simulated the mass transfer behavior in different regions of microvia surface (1000 rpm) and inner hole (100 rpm), respectively. It has been reported that the accelerator is predominant at the bottom of the microvia due to weak convection, while the suppressor and the leveler are synergistically predominant at the via opening and the board surface owing to strong convection during practical microvia electroplating process [38]. The change of cathodic deposition potential (η) is defined by this formula: $\Delta\eta = \eta$ (100 rpm)- η (1000 rpm), and it can be used to characterize the filling performance [38]. If the value is positive, a stronger convection will result in less copper deposition [38]. It can be seen from Fig. 2, after 1 ppm SPS is added into the base electrolyte, the $\Delta\eta_3$ become positive because of the different rotation speeds of Cu-RDE. Furtherly, the addition of 2 μmol/L DPP derivatives plays a positive role in improving the Δη as recorded in Fig. 3, and the cathodic deposition potential (η) immediately shifts to more negative values. At the same time, the change of cathodic deposition potential (η) is in the following order: $\Delta\eta_{p\text{-ClDPP-QAS}} < \Delta\eta_{FDPP\text{-}QAS} < \Delta\eta_{TDPP\text{-}QAS} < \Delta\eta_{SeDPP\text{-}QAS}$, the largest positive Δη value (13.8 mV) of SeDPP-QAS is obtained. The positive value of Δη showed that the rate of the copper deposition is inversely proportional to the strength of the forced convection [39,40]. Surprisingly, we find that the change of cathodic deposition potential is correlated negatively with the optical bandgap.

To further analyze the function of DPP derivatives in the additive system, potentiodynamic polarization curves of different derivatives were measured at 1000 rpm and the results are given in Fig. 4. With addition of 2 μmol/L different DPP derivatives, the

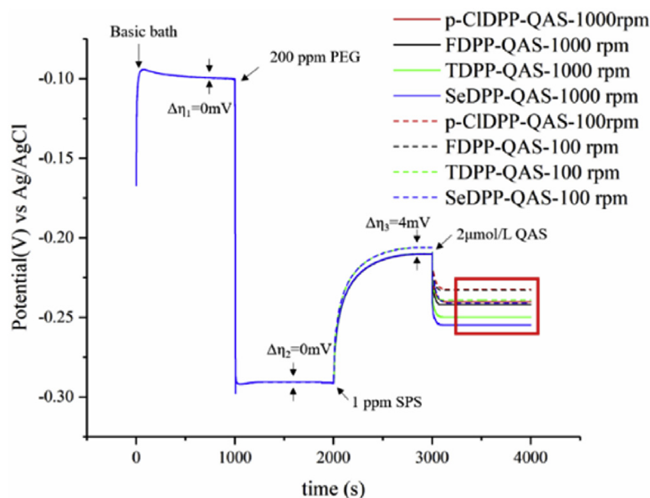

Fig. 2. GMs of plating solutions at the current density of 1.5 A/dm^2. Rotation speeds of Cu-RDE is 1000 and 100 rpm, PEG, SPS were injected into the basic bath at designed time. Four DPP derivatives were injected at 3000 s.

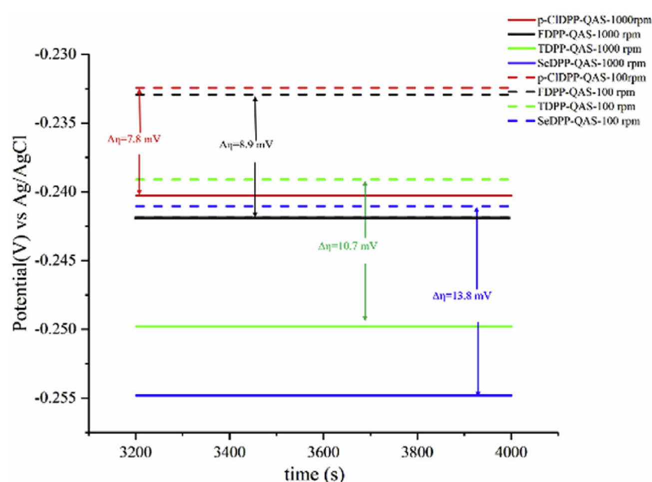

Fig. 3. Magnified view of the red box in Fig. 2.

Please cite this article as: K. Wang et al., Engineering aromatic heterocycle strategy: Improving copper electrodeposition performance via tuning the bandgap of diketopyrrolopyrrole-based leveler, Tetrahedron, https://doi.org/10.1016/j.tet.2019.130882

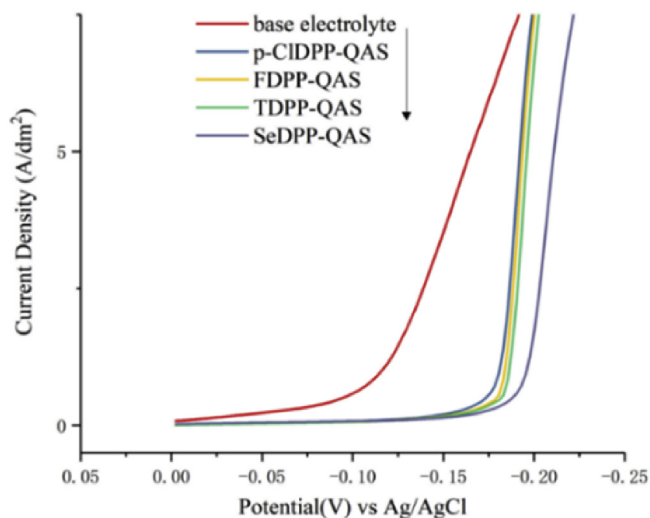

Fig. 4. Potentiodynamic polarization curves using 2 μmol/L DPP derivatives as the leveler in base electrolyte. The electrode rotation speed was 1000 rpm.

reductive currents shift to more negative value from −0.01 V versus Ag/AgCl electrode using the basic bath. This phenomenon suggested that the addition of DPP derivatives can increase the cathodic polarization. This inhibition can be attributed to the adsorption of DPP derivatives on the copper surface. According to Fig. 4, SeDPP-QAS exerts the greatest inhibiting effect (−0.18 V versus Ag/AgCl electrode) compared with other three quaternary ammonium salts [41].

3.2. Through-holes electroplating

Through-hole (TH) was used as the typical substrates of PCB to simulate the practical leveling performance. Four DPP derivatives was tested in the through-holes electroplating, the composition of the base electrolyte was 60 g/L $CuSO_4 \cdot 5H_2O$ and 200 g/L H_2SO_4, 1 ppm SPS, 200 ppm PEG. The cross-section of plated substrate of TH obtained from different baths were shown in Fig. 5.

Copper thickness in the center of TH is only about 10.02 μm and TP value is 43.5% when using bath with no leveler. Whereas, the injection of 2 μmol/L p-ClDPP-QAS, FDPP-QAS, TDPP-QAS and SeDPP-QAS made TP value increase to 75.6%, 85.2%, 88.7% and 98.8%, respectively (as displayed in Fig. 5 and the TP value is an approximation). It can be seen that the addition of 2 μmol/L SeDPP-QAS could effectively make the whole plating more uniform (marked in Fig. 5e). Moreover, the sidewall of the TH was flat after electroplating using the bath containing SeDPP-QAS. Besides, it is clearly indicated that the through-holes obtained from the bath containing DPP-QAS are thinner than the basic plating bath without DPP-QAS at the same plating conditions, this phenomenon also shows that the DPP-QAS leveler has well suppression performance.

3.3. Effect of DPP derivative on deposit morphology

Additionally, the influence of DPP-QAS on the surface morphology of copper deposit is investigated by FE-SEM, and the results are shown in Fig. 6. The surface micrograph of copper deposits is rough and consisted of relative large and coarse grains when using the base electrolyte without the DPP-QAS(shown in Fig. 6a). While the particle size decreases and the copper deposit became more uniform and flatter when using the electrolyte with 2 μmol/L DPP-QAS (shown in Fig. 6b–e). These phenomenon indicate that the DPP-QAS can be selectively adsorbed in the high current density areas and result in the leveling effect and the SeDPP-QAS has the best performance.

In order to analyze the leveling mechanism of an addition of DPP-QAS for electroplating Cu deposition, XRD of electrodeposition Cu films were performed, as shown in Fig. 7. Compared with the electrolyte without leveler, the (111) planes became dominant while the intensity of (220) decreased dramatically after added 2 μmol/L DPP derivatives. It indicated that DPP derivatives could inhibit the growth in the direction of the (220) planes and promote the (200) and (111) orientation. Besides, the SeDPP-QAS has the best performance among the four derivatives and the particle size is smaller than previous research examined by FE-SEM [26]. Formation of specific orientations in the presence of additives may result from the preferential adsorption of additive molecules onto particular facets [42]. One possible reason for the increased in (111) peak was that SeDPP-QAS preferentially occupied on the (111) facet and then effectively block the deposition of Cu onto these facets. Moreover, the intensity of the whole orientation peaks was obviously decreased due to the addition of SeDPP-QAS.

3.4. Photophysical properties

The obvious observed features in the absorption spectra of these

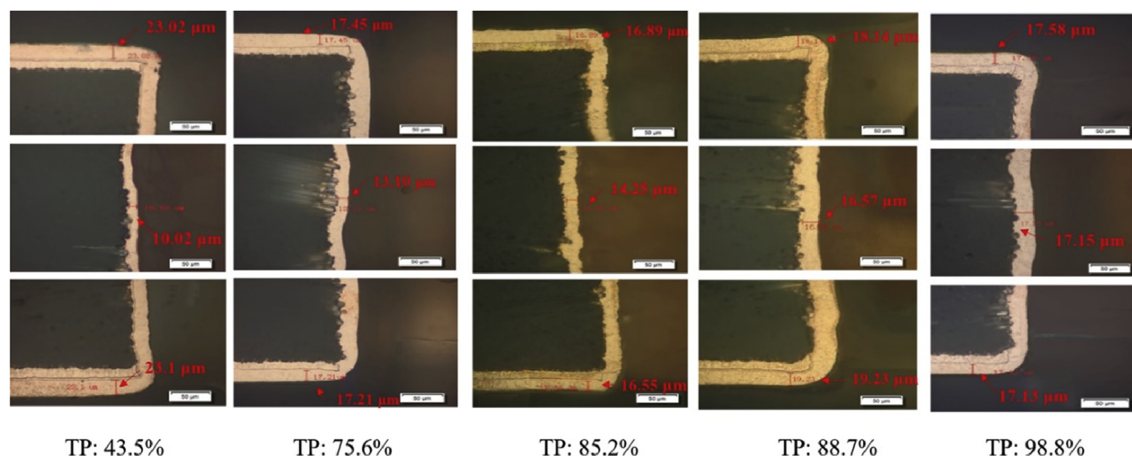

Fig. 5. Representative images of cross-section of TH obtained from the base electrolyte bath (a) without leveler, (b) with 2 μmol/L p-ClDPP-QAS, (c) with 2 μmol/L FDPP-QAS, (d) with 2 μmol/L TDPP-QAS and (e) with 2 μmol/L SeDPP-QAS.

Please cite this article as: K. Wang et al., Engineering aromatic heterocycle strategy: Improving copper electrodeposition performance via tuning the bandgap of diketopyrrolopyrrole-based leveler, Tetrahedron, https://doi.org/10.1016/j.tet.2019.130882

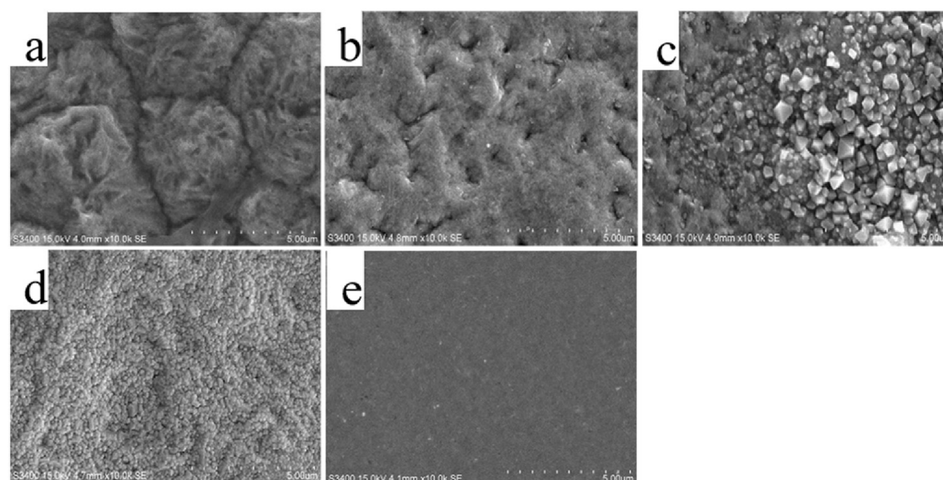

Fig. 6. FE-SEM images of copper deposits obtained in electrolyte: (a) base electrolyte, (b) containing the p-ClDPP-QAS leveler, (c) containing FDPP-QAS, (d) containing TDPP-QAS and (e) containing SeDPP-QAS.

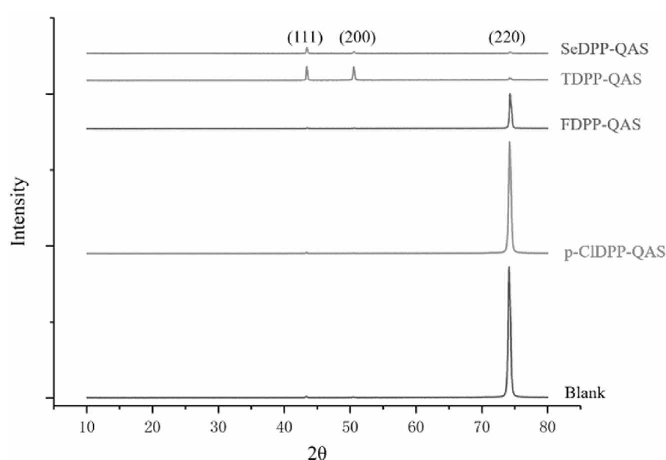

Fig. 7. XRD patterns of plated Cu films obtained in base electrolyte with or without 2 μmol/L DPP derivatives.

derivatives are shown in Fig. 8a. Firstly, we observe a gradual bathochromic shift of π-π* transition from p-ClDPP-QAS to FDPP-QAS, TDPP-QAS, SeDPP-QAS successively, indicating that furan, thiophene and selenophene as donor groups can decrease the bandgap in an increasing order [43]. The reason why SeDPP-QAS has the lowest optical bandgap compared with other DPP derivatives can be owing to the effect of selenium on lowering the LUMO energy level [31]. It also can be attributed to the decrease in aromaticity and increase in quinoidal character [28]. The ultraviolet−visible absorption spectra and the fluorescence spectra of these compounds can be found in Figs. 8a and 9a respectively. Photographs were taken to show the variation in the emitting behavior of the four different DPP derivatives under sunlight (Fig. 8b) and ultraviolet light (Fig. 9b) respectively. The quantum yields shown in Table S1 were calculated as curiosity because the solution looks bright under UV light illumination. We calculate the bandgap through the ultraviolet absorption and emission spectra as illustrated in Fig. S3. The pertinent data of the absorption and emission wavelength with the optical bandgap are summarized in Table 1. The optical bandgap obtained from experiment is compared with the theoretical bandgap obtained from theoretical calculation. Stokes shift and molar absorption coefficient are summarized in Table S2.

3.5. Quantum chemical calculations

The quantum chemical calculations are employed to obtain

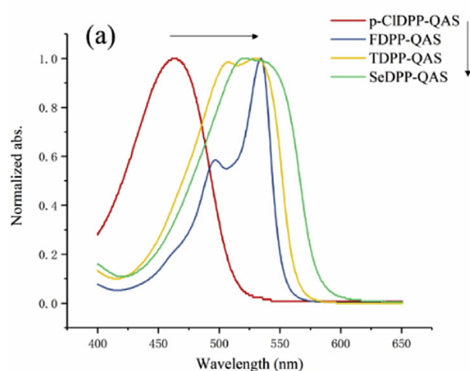

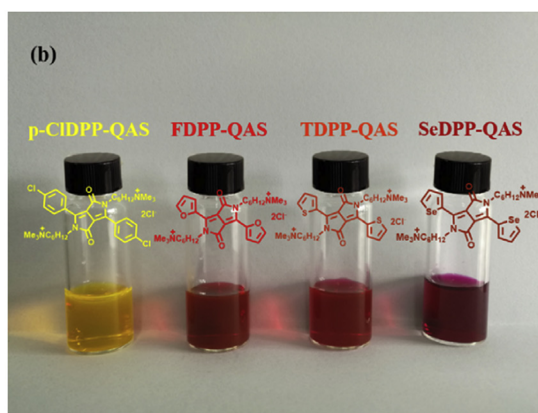

Fig. 8. (a) Absorption spectra of all targeted compounds in H_2O. (b) Photograph taken to show the variation in the emitting behaviors of the four different DPP-QAS under sunlight illumination.

Please cite this article as: K. Wang et al., Engineering aromatic heterocycle strategy: Improving copper electrodeposition performance via tuning the bandgap of diketopyrrolopyrrole-based leveler, Tetrahedron, https://doi.org/10.1016/j.tet.2019.130882

ARTICLE IN PRESS

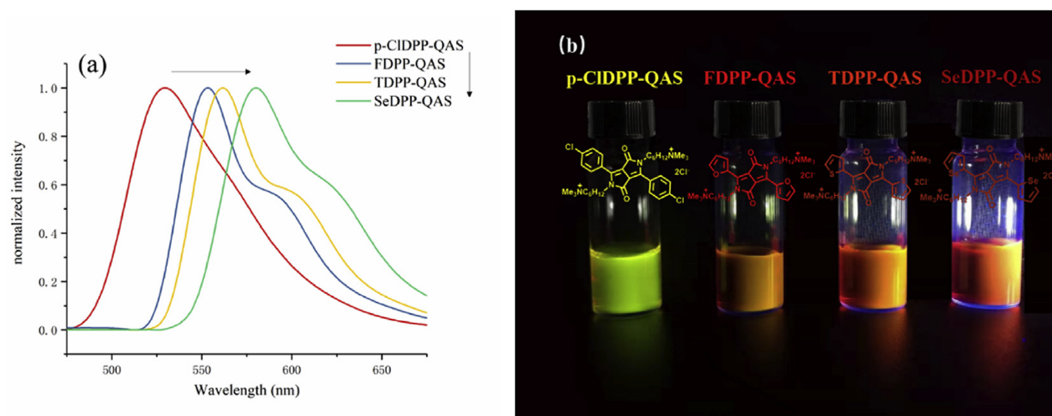

Fig. 9. (a) Emission spectra of all targeted compounds in H_2O. (b) Photograph taken to show the variation in the emitting behaviors of the four different DPP derivatives under UV light illumination (~365 nm).

Table 1
Summary of the photophysical data of the DPP derivatives in H_2O varied with different donor units.

Molecule	λ_{ab}(nm)	λ^{a}_{em}(nm)	Eg(eV)
p-ClDPP-QAS	463	529,561	2.48
FDPP-QAS	496,534	552,588	2.29
TDPP-QAS	506,530	562,595	2.26
SeDPP-QAS	520,537	580,618	2.2

[a] The excitation wavelength were the max absorption wavelength.

Table 2
Energy values of molecular orbital and bandgaps (ΔEg) of DPP derivatives.

DPP-QAS	E_{HOMO} (eV)	E_{LUMO} (eV)	ΔEg (eV)
p-ClDPP-QAS	−8.139	−5.268	2.871
FDPP-QAS	−8.039	−5.497	2.542
TDPP-QAS	−8.018	−5.507	2.511
SeDPP-QAS	−7.997	−5.522	2.475

some orbital information and electronic properties. The optimized geometries and electron density distribution in the HOMO and LUMO of the four DPP derivatives are shown in Fig. 10. As we expected, the HOMO energy of four DPP derivatives increased while the LUMO energy of four DPP derivatives decreased in the same order of: p-ClDPP-QAS, FDPP-QAS, TDPP-QAS and SeDPP-QAS as shown in Table 2. Since theoretical computation is based on hypothesis and approximation, the derived data may deviate from real values, so the HOMO value (Fig. S4) were measured by means of cyclic voltammetry and the data were shown in Table S3. The value of theoretical computation is lower than the experimental value getting from cyclic voltammetry. It is demonstrated that there are some deviations between the experimental value and the theoretical computation, mainly because the theoretical computation is calculated under vacuum condition, while the experimental value is obtained under solvent circumstance. Nevertheless, both the cyclic voltammetry results and the theoretical computation results has the same trend in HOMO and LUMO. The HOMO-LUMO gap are found to decrease in the order of p-ClDPP-QAS, FDPP-QAS, TDPP-QAS and SeDPP-QAS which is attributed to chalcogen atoms in DPP derivatives that can increase the HOMO energy and decrease the LUMO energy. The change of the band gap with different chalcogens could also be due to the molecular planarity which is affected by the aromatic heterocycle, then the dihedral angle data were showed in Fig. S6. The high torsional angle of p-ClDPP-QAS can be attributed to the six atoms of phenyl, while the torsional angle increased with the sequence of FDPP-QAS, TDPP-QAS and SeDPP-QAS may because of the increase of atomic radius. According to the frontier molecular orbital theory, the high E_{HOMO} and low E_{LUMO} represented that the molecule was easily to donate and accept electron. The adsorption ability of the organics on the metal surface would increase with the increase of E_{HOMO} and the decrease of E_{LUMO} [45]. This could be considered that lower bandgap additive gives rise to a stronger adsorption layer on the copper surface. This feature may increase the convection-dependent adsorption (CDA) [38], indicating that the additive with smaller bandgap may lead to stronger selective adsorption on high current density area. The selective adsorption usually results in large deposition potential change between the mouth and hole regions of through-hole PCB. Then it is reasonable to consider that the deposition potential change (Δη) value correlate negatively with the bandgap.

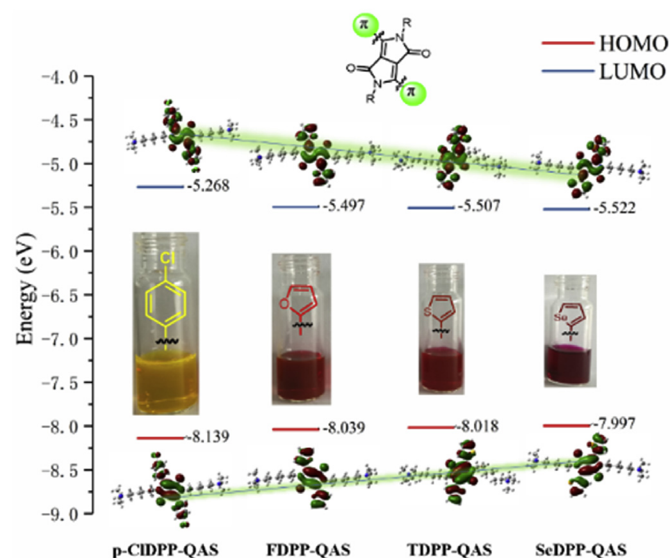

Fig. 10. Distributions and orbital energy values of the HOMO and LUMO of DPP derivatives.

The electrostatic potential (ESP) plot is a straightforward visualization of the preferred reaction sites and powerful tool for predicting molecular properties [21]. ESP plots map the distribution of electron density where positive ESP value corresponds to low

Please cite this article as: K. Wang et al., Engineering aromatic heterocycle strategy: Improving copper electrodeposition performance via tuning the bandgap of diketopyrrolopyrrole-based leveler, Tetrahedron, https://doi.org/10.1016/j.tet.2019.130882

ARTICLE IN PRESS

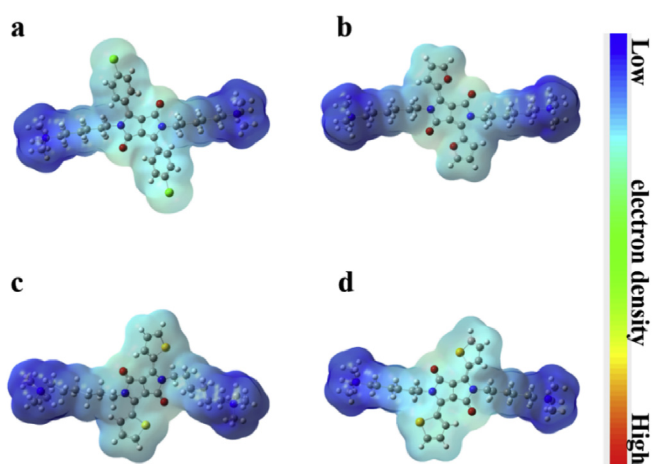

Fig. 11. ESP mapped of four DPP quaternary ammonium salts(a), p-ClDPP-QAS; (b), FDPP-QAS; (c), TDPP-QAS; (d), SeDPP-QAS.

electron density (blue color represents low electron density in Fig. 11). Fig. 11 demonstrates that the distribution of low electron density region of DPP derivatives is around the quaternary ammonium cations, indicating quaternary ammonium cations tend to be attracted to the copper surface where the electron density is high region during electroplating process. In addition, we can boldly speculate that the Cu^{2+} deposit on the copper surface process well prevented because of the planar structures of DPP derivatives.

3.6. Wetting performance

The wetting performance of electrolyte toward electrode is another important parameter since it can affect the speed of mass transfer in the practical copper electroplating process [44]. The contact angle(CA) of the electrolyte on the surface of copper broad is an important parameter to measure the wettability of the electrolyte. We conducted the electrolyte containing DPP derivatives contact angle (CA) test and the basic electrolyte was used as benchmark as shown in Fig. 12. The benchmark shows a larger CA about 71.5°, while the electrolyte containing DPP derivatives shows smaller CA of 64.3°, 59.4°, 52.8° and 48.1° for p-ClDPP-QAS, FDPP-QAS, TDPP-QAS and SeDPP-QAS derivatives, respectively. The small CA value implies that the heterocycle-modification of DPP leveler is able to tune the interface adsorption behavior which can further affects the practical copper electroplating. In particular, the CA of electrolyte containing SeDPP-QAS is smaller than the others indicating it has the best wettability on the copper surface.

3.7. Interaction between DPP derivatives and the copper surface

The adsorption behavior is investigated by XPS shown in Fig. S7. The detailed XPS peak of N1s is shown in Fig. 13b, integral areas of four derivatives are 344, 540, 798 and 978, respectively for p-ClDPP-QAS, FDPP-QAS, TDPP-QAS and SeDPP-QAS. The results indicate that the adsorption capacities of DPP derivatives on electroplated Cu surface are in the following order: p-ClDPP-QAS < FDPP-QAS < TDPP-QAS < SeDPP-QAS, which is in agreement with the Cu deposition potential with addition of DPP derivatives obtained from electrochemical evaluations (Figs. 1–4) [45]. Moreover, we compared the XPS profiles of DPP compounds absorbed on Cu surface with their pure bulk state as shown in Fig. 13a, the shape of nitrogen changes from two narrow peaks (the binding energy of 399.9 eV could be assigned to the nitrogen atoms of amides. The peak at the binding energy of 402.2 eV could be belonged to the quaternary nitrogen atoms) to one broad peak, the changed shape of the nitrogen peak demonstrate that nitrogen is the main binding atoms in their chemical structures. DPP derivatives bear two quaternary ammoniums and two symmetric heterocyclic groups. Hence, it can strongly adsorb on the cathodic surface, particularly on protrusion with high electron density during electroplating [46]. These characteristics indicate that DPP derivatives can be used as a leveler for the TH electroplating.

4. Conclusions

Four DPP-based quaternary ammonium salts with different aromatic rings were synthesized and the reasons for different inhibition abilities in electroplating process are investigated by electrochemical analysis, DFT, CA and XPS. The main findings are summarized as follows:

i.) An excellent leveler is reported for through-hole copper electroplating, namely SeDPP-QAS.

ii.) It is found that the E_{HOMO} of DPP derivatives increases following the order: $E_{p\text{-ClDPP-QAS}} < E_{FDPP\text{-}QAS} < E_{TDPP\text{-}QAS} < E_{SeDPP\text{-}QAS}$, while the E_{LUMO} decreases following the order: $E_{p\text{-ClDPP-QAS}} > E_{FDPP\text{-}QAS} > E_{TDPP\text{-}QAS} > E_{SeDPP\text{-}QAS}$,

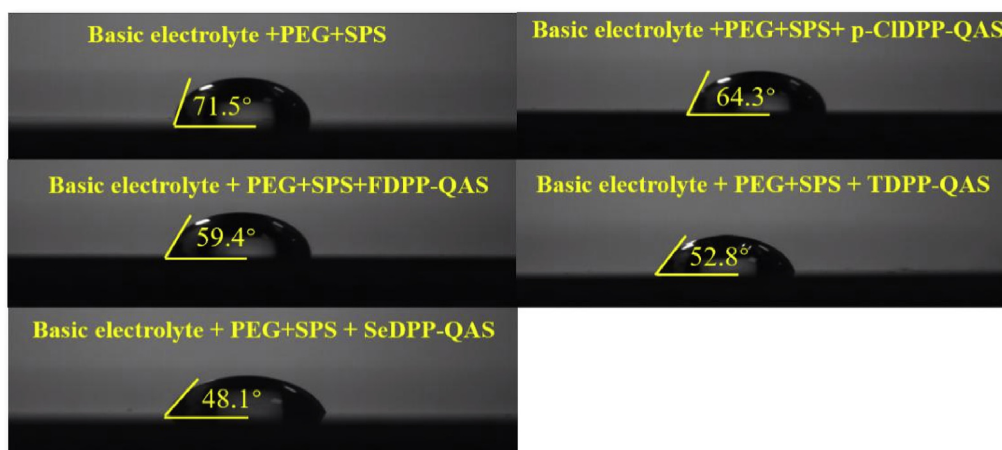

Fig. 12. The contact angle of basic electrolyte with 1 ppm SPS and 200 ppm PEG containing various DPP derivatives at the concentration of 2 μmol/L.

Please cite this article as: K. Wang et al., Engineering aromatic heterocycle strategy: Improving copper electrodeposition performance via tuning the bandgap of diketopyrrolopyrrole-based leveler, Tetrahedron, https://doi.org/10.1016/j.tet.2019.130882

ARTICLE IN PRESS

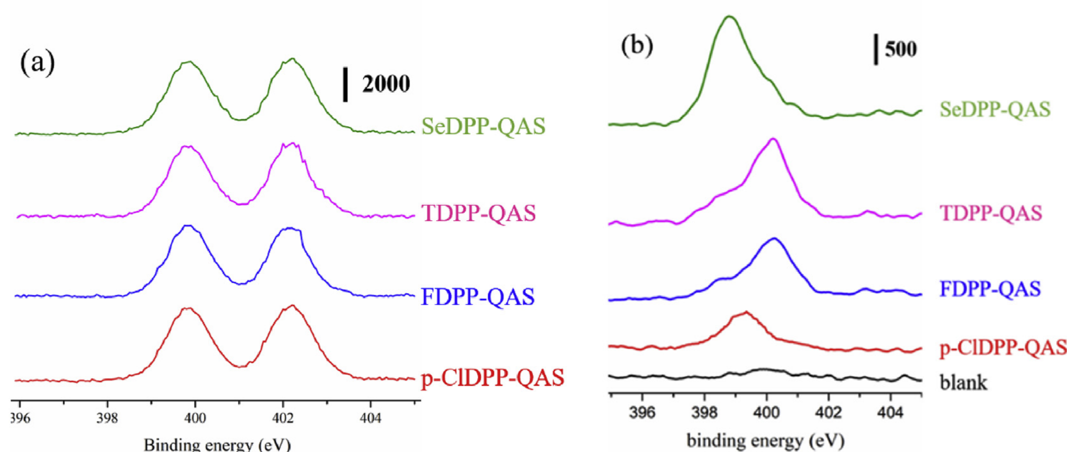

Fig. 13. (a) High resolution N1s peaks of DPP derivatives pure bulk state, (b) High resolution N1s peaks of DPP derivatives adsorbed on copper surface.

Consequently, the energy of bandgap decreases following the order: $\Delta E_{p\text{-ClDPP-QAS}} > \Delta E_{FDPP\text{-QAS}} > \Delta E_{TDPP\text{-QAS}} > \Delta E_{SeDPP\text{-QAS}}$.

iii.) The comprehensive electrochemical evaluation demonstrated that the largest deposition potential change ($\Delta\eta$) increases following the order: p-ClDPP-QAS < FDPP-QAS < TDPP-QAS < SeDPP-QAS.

iv.) Quantum chemical calculations and electrochemical evaluation indicate that the energy gap (ΔE) of DPP derivatives correlate negatively with the deposition potential change $\Delta\eta$.

v.) The impact of chemical structure on bandgap is studied. It is an effective way to tune the bandgap by changing the aromatic rings and the attachment of chalcogen atoms has a further effect on the plating inhibition performance.

Declaration of competing interest

The authors declared that they have no conflicts of interest to this work.

We declare that we do not have any commercial or associative interest that represents a conflict of interest in connection with the work submitted.

Acknowledgement

This research was financially supported by the National Natural Science Foundation of China (21772039, 21272069), and we gratefully acknowledge financial support from the Central Universities and Key Laboratory of Organofluorine Chemistry, Shanghai Institute of Organic Chemistry, Chinese Academy of Sciences. Support from the Chinese Scholarship Council is also acknowledged.

Appendix A. Supplementary data

Supplementary data to this article can be found online at https://doi.org/10.1016/j.tet.2019.130882.

References

[1] Y. Chen, W. He, X. Chen, C. Wang, Z. Tao, S. Wang, et al., Electrochim. Acta 120 (2014) 293.
[2] S. Yang, Z. Thacker, E. Allison, M. Bennett, N. Cole, P.J. Pinhero, ACS Appl. Mater. Interfaces 9 (2017) 40921.
[3] J.J. Hatch, M.J. Willey, A.A. Gewirth, J. Electrochem. Soc. 158 (2011) D323.
[4] C. Chang, X. Lu, Z. Lei, Z. Wang, C. Zhao, Electrochim. Acta 208 (2016) 33.
[5] Z. Lai, S. Wang, C. Wang, Y. Hong, Y. Chen, H. Zhang, et al., Electrochim. Acta 273 (2018) 318.
[6] M. Tang, S. Zhang, Y. Qiang, S. Chen, L. Luo, J. Gao, et al., RSC Adv. 7 (2017) 40342.
[7] M.H. Lee, Y. Lee, J.H. Oh, Y.G. Kim, S.K. Cho, J.J. Kim, J. Electrochem. Soc. 164 (2017) D1051.
[8] H.P. Zhu, Q.S. Zhu, X. Zhang, C.Z. Liu, J.J. Wang, J. Electrochem. Soc. 164 (2017) D645.
[9] W.P. Dow, C.C. Li, M.W. Lin, G.W. Su, C.C. Huang, J. Electrochem. Soc. 156 (2009) D314.
[10] A.-Y. Wang, B. Chen, L. Fang, J.-J. Yu, L. Wang, Electrochim. Acta 108 (2013) 698.
[11] C. Wang, J. Zhang, P. Yang, M. An, Electrochim. Acta 92 (2013) 356.
[12] J. Xu, S. Bi, W. Tang, Q. Kang, D. Niu, S. Hu, et al., J. Mater. Chem. A 7 (2019) 18100.
[13] K. Nie, B. Dong, H. Shi, L. Chao, X. Duan, X. Jiang, Dyes Pigments 160 (2019) 814.
[14] S. Bi, G. Zhang, Y. Wu, S. Wu, L. Wang, Dyes Pigments 134 (2016) 586.
[15] G. Zhang, H. Li, S. Bi, L. Song, L. Lu, L. Zhang, et al., J. Analyst 138 (2013) 6163.
[16] G. Zhang, S. Bi, L. Song, F. Wang, J. Yu, L. Wang, Dyes Pigments 99 (2013) 779.
[17] S. Stas, J.Y. Balandier, V. Lemaur, V. lemaur, O. Fenwick, G. Tregnago, et al., Dyes Pigments 97 (2013) 198.
[18] S. Qu, H. Tian, J. Chem. Commun. 48 (2012) 3039.
[19] Luňák Stanislav Jr., M. Vala, Jan Vyňuchal, et al., Dyes Pigments 101 (2011) 269.
[20] H. Liang, X. Zhang, R. Peng, X. Ouyang, Z. Liu, S. Chen, et al., Dyes Pigments 112 (2015) 145.
[21] Y. Li, P. Sonar, L. Murphy, W. Hong, Energy Environ. Sci. 6 (2013) 1684.
[22] T.R. Hong, J. Shin, H.A. Um, et al., Dyes Pigments 108 (2014) 7.
[23] L. Dou, J. You, J. Yang, C.-C. Chen, Y. He, S. Murase, et al., Nat. Photonics 6 (2012) 180.
[24] L. Dou, W.-H. Chang, J. Gao, C.-C. Chen, J. You, Y. Yang, Adv. Mater. 25 (2013) 825.
[25] B. Chen, J. Xu, L. Wang, L. Song, S.J. Wu, ACS Appl. Mater. Interfaces 9 (2017) 7793.
[26] J. Xu, B. Chen, J. Lv, D. Chang, D. Niu, S. Hu, et al., Dyes Pigments 170 (2019) 107559.
[27] A.B. Pun, L.M. Campos, D.N. Congreve, J. Am. Chem. Soc. 141 (2019) 3777.
[28] F. Fringuel, G. Marino, A. Taticchi, G. Grandoli, J. Chem. Soc., Perkin Trans. 2 (1974) 332.
[29] J. Dhar, T. Mukhopadhay, N. Yaacobi-Gross, T.D. Anthopoulos, U. Salzner, S. Swaraj, S.J. Patil, Phys. Chem. B 119 (2015) 11307.
[30] S. Munazza, M. Thomas, L. John, R. Stephan, B.D. Ester, E. Scott, et al., Chem. Sci. 3 (2012) 181.
[31] J. Dhar, N. Venkatramaiah, A. Anitha, S. Patil, J. Mater. Chem. C 2 (2014) 3457.
[32] W.J. Hehre, R. Ditchfield, J.A. Pople, J. Chem. Phys. 56 (1972) 2257.
[33] C. Lee, W. Yang, R.G. Parr, Phys. Rev. B Condens. Matter Mater. Phys. 37 (1988) 785.
[34] A. Kokalj, S. Peljhan, Langmuir 26 (2010) 14582.
[35] J.F. Wei, B. Han, Q. Guo, X.Y. Shi, W.L. Wang, N. Wei, Angew. Chem. 122 (2010) 8385.
[36] P.K. Chattaraj, S. Giri, Annu. Rep. Prog. Chem. Sect. C Phys. Chem. 105 (2009) 13.
[37] H.O. Villar, P. Otto, M. Dupuis, J. Ladik, J. Synth. Metals 59 (1993) 97.
[38] W.-P. Dow, H.-S. Huang, M.-Y. Yen, H.-C. Huang, J. Electrochem. Soc. 152 (2005) C425.
[39] C. Wang, J. Zhang, P. Yang, M. An, Electrochim. Acta 92 (2013) 356.

ARTICLE IN PRESS

[40] W.-P. Dow, C.-W.E. Liu, J. Electrochem. Soc. 153 (2006) C190.
[41] C. Liao, S. Zhang, S. Chen, Y. Qiang, G. Liu, M. Tang, B. Tan, D. Fu, Y. Xu, J. Electroanal. Chem. 827 (2018) 151.
[42] Y.J. Han, X. Zhang, G.W. Leach, Langmuir 30 (2014) 3589.
[43] E.E. Havinga, W. Ten Hoeve, H. Wynberg, J. Synth. Metals 55 (1993) 299.
[44] J. Zhang, W. Luo, Y. Li, L. Gao, M. Li, Appl. Surf. Sci. 359 (2015) 736.
[45] Z. Lei, L. Chen, W. Wang, Z. Wang, Z. Zhao, Electrochim. Acta 178 (2015) 546.
[46] C. Wang, J. Zhang, P. Yang, B. Zhang, M. An, J. Electrochem. Soc. 160 (2013) D85.

Please cite this article as: K. Wang et al., Engineering aromatic heterocycle strategy: Improving copper electrodeposition performance via tuning the bandgap of diketopyrrolopyrrole-based leveler, Tetrahedron, https://doi.org/10.1016/j.tet.2019.130882